COMMUNICATIONS IN SCIENCE AND TECHNOLOGY
Homepage: cst.kipmi.or.id

Fabrication and photocatalytic performance of ZnO-biochar composites for eliminating dye waste

Desi Heltina[a,*], Danil Yoselino[a], Nabellia[a], Agustina Dumaria[a], Khairati Amila[a], Komalasari[a], Maria Peratenta.S[a], Amun Amri[a], Zhong Tao Jiang[b]

[a]*Department of Chemical Engineering, Universitas Riau, Pekanbaru 28293, Indonesia*
[b]*Surface Analysis and Material Engineering Research Group, Murdoch University, Western Australia 6150, Australia*

Article history:
Received: 29 September 2025 / Received in revised form: 29 November 2025 / Accepted: 30 November 2025

Abstract

The synthesis of the ZnO-biochar composite from palm kernel shell biomass waste has been accomplished through the utilization of the solvothermal method, yielding a satisfactory outcome. The resulting composite, a combination of ZnO and biochar, has been utilized in the degradation of methylene blue waste compounds. The objective of this research is to synthesize ZnO-biochar composites from palm shells, and to determine the optimal solvothermal temperature and duration. This research was initiated with the preparation of palm shells into biochar. Subsequently, the ZnO-biochar composite was synthesized with variable solvothermal temperatures and solvothermal times. The ZnO-biochar composite was characterized using analytical techniques including SEM-EDX, FT-IR, XRD, BET and UV-vis DRS. The most effective degradation of methylene blue was exhibited by the ZnO-biochar composite sample synthesized at a solvothermal temperature of 180˚C and a solvothermal time of 10 hours, achieving a degradation of 88.29%. The enhanced photodegradation performance of this composite sample is attributed to its high surface area, capacity for visible light absorption, and the dimensions of the active crystals, which can account for the high performance of the ZnO-biochar composite for photocatalytic degradation.

Keywords: ZnO, biochar; photodegradation; palm kernel shell; methylene blue

1. Introduction

Liquid waste has become the most significant cause of environmental pollution. The presence of untreated and unmanaged liquid waste has been demonstrated to exert a detrimental effect on water bodies, with a particular emphasis on water resources [1]. Textile waste is one of the most abundant forms of liquid waste. Data from the Central Bureau of Statistics in 2022 revealed that the demand for dyes in both the production process and the industry increases each year. The textile industry utilizes synthetic dyes that are characterized by their resistance to degradation, thus necessitating additional treatment [2]. The dye content is constituted of organic substances, component complexity, high color intensity; therefore, its presence in waste water can hinder the process of decomposition [1].

The research employed methylene blue as the synthesized dye due to its favorable solubility in water and affordability. The heterocyclic aromatic compound, also known as methylene blue, is characterized by a planar structure with a molecular weight of 319.85 g/mol and chemical formula of $C_{16}H_{18}N_3SCl$ [3]. The presence of methylene blue in wastewater streams has been demonstrated to create multiple health risks, including cyanosis, damage to body tissue or cell, puke, dizzy, shock and increased heart rate as well as multiple additional conditions [3]. The photodegradation process that utilizes photocatalytic semiconductor materials has been shown to be an effective method for the treatment of methylene blue dye waste. The utilization of semiconductor photocatalysts provides three main benefits as they preserve structural stability while being affordable and non-toxic [4]. The process of photocatalysis occurs when a solid catalyst interacts with another material through ultraviolet radiation energy. The process of photocatalysis facilitates the reaction of materials with each other through solid catalysts when exposed to ultraviolet radiation [5]. Environmental treatment of problems becomes possible through photodegradation when semiconductors act as catalysts in economical processes. The photodegradation of organic pollutants in wastewater can be facilitated by the utilization of semiconductors, such as ZnO and WO_3 and CdS and Bi_2WO_6

* Corresponding author.
Email: desi.heltina@lecturer.unri.ac.id
https://doi.org/10.21924/cst.10.2.2025.1795

and BiOCl. The treatment of wastewater through the degradation of organic pollutant becomes possible using specific semiconductors including ZnO and WO_3 as well as CdS and Bi_2WO_6 and BiOCl [6]. Zinc oxide (ZnO) is a material utilized widely in a variety of applications in daily life. In addition to its cost-effectiveness, abundance, and non-toxic nature, it is a material of significant commercial importance. ZnO is a semiconductor that exhibits a large band gap, high thermal conductivity, and rapid electron mobility in which these properties offer numerous advantages for photocatalytic applications. It is one of the essential metal oxides for technological materials and has a wide range of applications due to its unique chemical and physical properties, encompassing outstanding chemical stability, an elevated electrochemical coupling coefficient, broad-spectrum radiation absorption, and exceptional photostability [7]. However, ZnO in its pure form exhibits a band gap of approximately ~3.2 eV, which is substantial and consequentlyreduces its effectiveness under UV light. A potential approach involves the modification of ZnO with carbon-based materials [7]. Carbon doping in ZnO has been demonstrated to have the potential to shift the absorption spectrum of ultraviolet light towards the visible light region [6].

Pyrolysis refers to an endothermic reaction [7] that converts biomass into products, including char (solid carbon), gases such as methane or hydrogen, and bio-oil (liquid product), in the absence of oxygen through rapid heating. The process parameters that influence biochar production include pressure, temperature, reaction time, and particle size. Furthermore, the operating conditions determine both the quantity of charcoal produced and the quality characteristics of the pyrolysis output. It has been demonstrated that the efficiency of biochar production is reduced when pyrolysis occurs at elevated temperatures and with increased heating rates. The production of liquid products is more probable when gas residence times are short, and temperatures are low and heating rates are high. The production of gaseous products is increased by extending gas residence times, elevating temperatures and decreasing heating rates. The duration of residence determines both the quantity of biochar produced and the development of biochar characteristics through pore formation at different scales. Research finding indicated that an increase in gas residence times results in the formation of charcoal with larger pore dimensions [8]. Scientists have proven that peanut shell biomass waste can be utilized as an effective material in the creation of biochar graphene-like nanocomposites, thereby enhancing photocatalytic activity [9]. The primary components of palm kernel shell biomass are lignin (48%), cellulose (30%), and hemicellulose (22%) [10]. The high content of lignin and cellulose in peanut shells and palm kernel shells renders palm kernel shells an excellent candidate for biochar production.

The research creates a photodegradable material for methylene blue dye through a ZnO-biochar composite made from palm kernel shell biomass. It evaluates how solvothermal temperature and time duration affect the surface area and crystal size as well as the visible light absorption properties of the material. The research findings will facilitate the development of an efficient photocatalytic system for the degradation of toxic compound in liquid solutions by scientists. The utilization of palm kernel shells in the production of biochar constitutes a waste management solution to the palm oil industry while reducing their waste output.

2. Materials and Methods

2.1. Materials

The experimental research study employed palm kernel shells as biomass, in conjunction with zinc nitrate hexahydrate ($Zn(NO_3)_2 \cdot 6H_2O$, AR) and glacial acetic acid and ethanol (EtOH) and methylene blue (MB, 98%) as chemical and solvent substances.

2.2. Pretreatment of palm kernel

The surface contaminants of palm kernel shell biomass (PKS) were removed through water washing prior to drying at 80˚C and subsequent crushing and 100-mesh sieve screening.

2.3. Synthesis of ZnO-biochar composites

The hydrothermal method, in conjunction with calcination treatment, enabled researchers to fabricate composite materials consisting of ZnO and biochar. The preparation of the acidic solution necessitated the dissolution of 3.6560 grams of $Zn(NO_3)_2 \cdot 6H_2O$ and 2 mL of glacial acetic acid in 40 mL of ethanol. It is evident that adequate stirring of the processed palm kernel shell (PKS) was achieved, thereby ensuring complete dispersion in the solution. The system was transferred to an autoclave for temperature control at 150˚C, 160˚C, 170˚C and 180˚C while maintaining different solvothermal times of 8, 10 and 12 hours. Subsequently, the solid precursor was obtained through a process of centrifugation and thoroughly dried in an oven. Afterwards, the dried precursor was calcined at 700˚C under a nitrogen atmosphere for 2 hours to produce the ZnO and palm kernel shell composite.

2.4. Characterization

The morphologies, elemental compositions, and elemental mapping of the samples were examined using a scanning electron microscope (SEM, JEOL JSM-6510LA) operated at an accelerating voltage of 20 kV and a magnification scale of 5 µm. The functional groups present in the nanocomposite were characterized by Fourier-transform infrared (FTIR) spectroscopy. The (FTIR) spectrophotometer (PerkinElmer Spectrum IR, version 10.6.1) was utilized within the wavelength range of 4000–400 nm. The specific surface area was determined using the Brunauer–Emmett–Teller (BET) method with a surface area analyzer (Quantachrome NovaTouch LX4). Prior to measurement, the samples were degassed under vacuum at 300°C for 3h. The characterization analysis for crystal structures was conducted using X-ray diffraction (XRD, Bruker D2) operated at 30 mA and 40 kV with Cu Kα radiation and a scan rate of 2° min^{-1}. and 40 kV with Cu Kα radiation and a scan rate of 2° min^{-1}. UV–Vis

diffuse reflectance spectroscopy (UV–Vis DRS) was employed to determine the band gap energy of the synthesized ZnO–biochar photocatalyst within the wavelength range of 420-800 nm.

2.5. Photocatalytic test

The ZnO-Biochar composite, with a mass of 40 mg was mixed in 300 mL with a methylene blue of 10 ppm. The experiment was conducted within a photodegradation reactor (40 x 50 x 60 cm) for 30 minutes with the lamp deactivated and under a mercury lamp (Philips, 250 Watt) for 150 minutes. The concentration of methylene blue following degradation was determined by means of a UV-vis spectrophotometer in accordance with the SNI 06-6989.21-2004 technique. The photodegradation activity of methylene blue was calculated using the following equation:

$$Photodegradation\ Efficiency\ (\%) = \frac{C_0 - C}{C_0} \times 100\% \qquad (1)$$

3. Results and Discussion

3.1. Photocatalytic performances

Prior to the photocatalytic test, a dark control experiment was performed by introducing the ZnO–biochar composite into a methylene blue solution and maintaining the mixture in the absence of light for 30 minutes. The objective of the present study was to conduct this procedure to examine degradation without any light exposure. The experiment comprised two stages. Firstly, a dark control period was conducted from -30 to 0 minutes, and subsequently, a photocatalytic test was performed from 0 to 150 minutes as illustrated in Fig. 1. The dark control experiment demonstrated a negligible decline in methylene blue concentration, attributable to surface absorption effects. The absence of illumination resulted in the failure to form electron–hole pairs, which are prerequisite for the initiation of photocatalytic reactions. [11]. It has been demonstrated that both biochar and activated carbon possess the capability to adsorb methylene blue through physical interactions as well as their extensive surface areas [12]. Consequently, the negligible decline in methylene blue concentration observed during the dark control stage can be attributed solely to physical adsorption, rather than photocatalytic degradation.

As demonstrated in Fig. 1, the degradation experiment was conducted within the time range of 0 to 150 minutes under illumination. In comparison to the dark control condition, all samples exposed to light demonstrated a significantly higher rate of degradation. The composite carbonized for 10 hours exhibited the highest degradation efficiency, indicating that charge separation was more effective and electron–hole recombination was effectively suppressed. Previous studies by Shrestha et al. [13] and Jing et al. [12] have demonstrated that the presence of carbon facilitated electron transfer and reduced the recombination of electron–hole pairs, thereby enhancing photocatalytic activity.

As depicted in Fig. 1, the percentage decrease in concentration increases with increasing solvothermal temperature. The percentage reduction in methylene blue concentration in the ZnO-biochar composite at a solvothermal temperature of 180˚C is superior to that at a temperature of 150˚C. The percentage concentration produced is influenced by differences in surface area and band gap energy. It is evident from the analysis of the BET and UV-vis DRS characteristics obtained that the enhancement in the photocatalytic activity of the composite is attributable to the increase in the number of hole-electron pairs resulting from the reduction in the band gap energy [15]. The surface area of composite has been demonstrated to have a significant impact on the magnitude of their photocatalytic performance. The greater surface area facilitates increased contact between pollutants, allowing for the degradation of a greater number of organic compounds. Consequently, surface area emerges as a pivotal factor in the methylene blue degradation process [9].

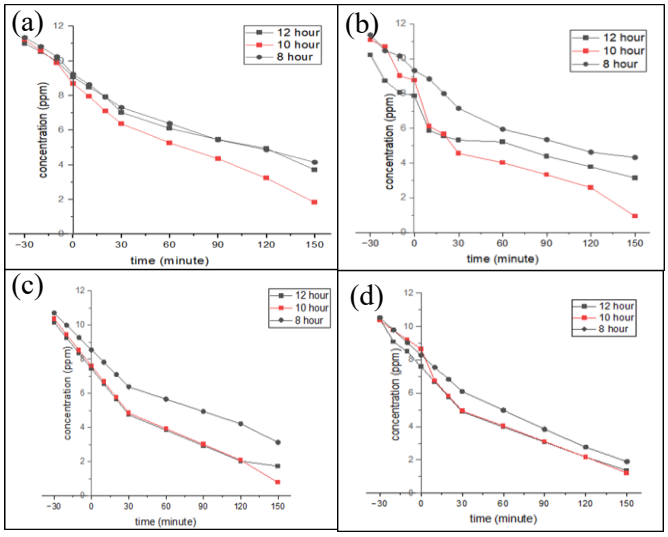

Fig. 1. Evaluation of the ZnO-biochar composite's effectiveness in methylene blue degradation at temperature (a) 150°C; (b) 160°C; (c) 170°C; (d) 180°C

Based on the obtained photodegradation results, an increase in reaction temperature led to higher photodegradation efficiency. Research studies have demonstrated that elevating the temperature of solvothermal synthesis leads to enhanced photocatalytic results [16]. Research studies have demonstrated that the production of ZnO materials at elevated temperatures has been shown to result in the enhancement of diffraction peak sharpness. This process has been observed to lead to an increase in surface area and a decrease in band gap energy. Consequently, this has been found to result in superior methylene blue degradation performance [17]. Similarly, studies on biochar-supported ZnO have demonstrated that elevated synthesis temperatures improve ZnO dispersion on the biochar surface, thereby producing a greater number of active sites for photoreactions [18].

The photodegradation results indicated that an increase in solvothermal reaction time results in enhanced photodegradation effectiveness. This finding aligns with the conclusions of other studies, which suggest that prolonging the duration of the solvothermal process can enhance photocatalytic activity to a certain extent. It is imperative to extend the reaction time to facilitate the deposition and

development of structures possessing large surface areas and enhanced photoactivity. The percentage of degradation increased from 4 to 24 hours and then decreased at 36 hours using the TPTZ (2,3,5-triphenyltetrazoliumchloride)-TiO_2 composite [19].

The composite obtained in this study exhibited significantly enhanced properties in comparison to pure ZnO. The comparison of the degradation of methylene blue using the ZnO-biochar composite, ZnO, and a control without the ZnO-biochar composite is presented in Fig. 2.

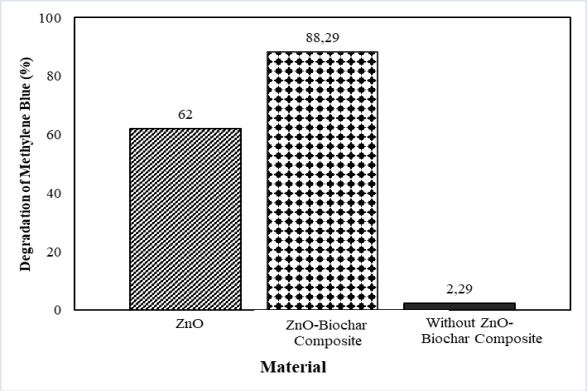

Fig. 2. Comparison of performance test of pure ZnO, ZnO-biochar composite and without ZnO-biochar composite for methylene blue degradation

As illustrated in Fig. 2, the degradation of methylene blue was found to be 62% using ZnO, while the degradation using ZnO-biochar at a solvothermal temperature of 180˚C and a reaction time of 10 hours was 88.29%. In contrast, the degradation without the ZnO-biochar composite was found only to be 2.29%. These results obtained from this study suggest that the functional groups present in biochar have the capacity to create numerous active sites for the adsorption of Zn^{2+} ions, thereby facilitating the formation of ZnO composites. The findings of this study are in alignment with those of Wang's research, which states that the functional groups present in biomass can enhance the adsorption of Zn^{2+} ions on the biomass surface, thereby promoting the in-situ conversion to ZnO [19].

Control experiments revealed that photolysis of methylene blue under UV light without any photocatalyst resulted in only 3.12% degradation after 150 minutes. Concurrently, the dark control exhibited negligible change (<1%). These obtained results confirm that the significant degradation observed in ZnO-biochar composites is primarily due to photocatalytic activity rather than natural photolysis or adsorption.

As demonstrated in Fig. 3, the percentage decrease in concentration increased with increasing solvothermal temperature. The ZnO-biochar composite exhibited superior methylene blue concentration reduction when synthesized at 180°C in comparison to 150°C. The disparity in observed outcomes can be attributed to different band gap energies and surface areas of the composite material. As the band gap energy decreases, there is an observed increase in the number of hole-electron pairs, which consequently leads to an enhancement in the photocatalytic performance of the composite material [19]. The photocatalytic activity of the composite material depends heavily on its surface area dimensions. The surface area is a determining factor in the extent of contact between pollutants and the composite material, which in turn has a significant impact on the efficiency of organic compound degradation. The degradation of methylene blue depends heavily on the surface area of the material [9].

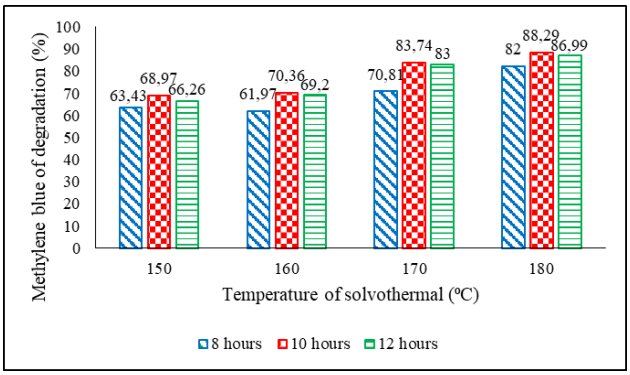

Fig. 3. Effect of temperature and time of solvotermal on the ZnO-biochar composite performance to methylene blue degradation

3.2. Characterization of ZnO-biochar composite

3.2.1. Scanning electron microscopic-energy dispersive X-Ray (SEM-EDX)

The Scanning Electron Microscopy (SEM) technique was utilized to examine the microstructure of ZnO-biochar composite materials. The primary objective of the SEM analysis was to examine the physical appearance of ZnO-biochar materials.

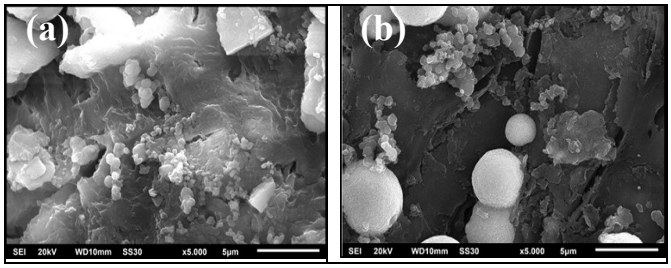

Fig. 4. Scanning electron microscope (SEM) images of (a) ZnO-biochar without pyrolysis; (b) ZnO-biochar composites with pyrolysis (180ºC; 10 hours)

As illustrated in Fig. 4(a), the non-pyrolyzed ZnO-biochar material exhibits a paucity of pores. However, Fig. 4(b) demonstrates that pyrolysis results in more extensive pore structures. The research findings of Leichtweis lend support to this outcome as pyrolysis of ZnO-biochar produces materials with an average pore size of 1.57 nm [20]. Furthermore, Fig. 4(b) reveals that the ZnO-biochar composite (180°C; 10 hours) possesses a porous structure, with spherical ZnO particles present on the surface resembling graphene [20]. In the ZnO-biochar composite (180°C; 10 hours), ZnO was distributed on the graphene-like surface [20]. A comparable finding was demonstrated by Yu, indicating that ZnO at a solvothermal temperature of 180°C has a spherical morphology [21].

Subsequent to the analysis of the composite's morphology via SEM, Energy Dispersive X-Ray (EDX) testing was conducted to ascertain the mass percentage of components in ZnO-biochar. The results of the EDX analysis for ZnO-biochar (180°C; 10 hours) are presented in Table 1.

Table 1. Constituent elements of ZnO-biochar composites (180ºC; 10 hours)

Element	(% atom)
C	84.86
O	10.81
Zn	4.13

As illustrated in Table 1, the ZnO-biochar composites (180°C; 10 hours), consist of carbon (C), oxygen (O), and zinc (Zn) components. The Zn and O elements represent the ZnO compound, and the carbon represents the biochar precursor. The presence of C, O, and Zn components in the composite indicates that the ZnO-biochar composite has been successfully synthesized from palm kernel shell biomass waste and ZnO.

3.2.2. Brunauer-emmett-teller (BET) analysis

The performance of the photocatalysis process is affected by a number of factors, including the specific surface area. A key objective of synthesizing ZnO-biochar composites is to enhance the surface area of ZnO. The specific surface area of a sample can be determined by means of BET (Brunauer-Emmett-Teller) analysis. A comparison of the surface area for several samples can be seen in Table 2.

Table 2. Surface area of ZnO-biochar composites

Material	Surface area (m^2/g)
*Pure ZnO	34.77
ZnO-biochar (150ºC; 10 hours)	68.60
ZnO-biochar (180ºC; 10 hours)	103.16
ZnO-biochar (180ºC; 12 hours)	101.51

(Source: *[17])

As illustrated in Table 2, the addition of biochar increases the surface area of the ZnO photocatalyst. This finding aligns with other research indicating that graphene sheets, which possess a large surface area, positively influence the performance of ZnO photocatalysts in the photodegradation process [22]. The ZnO-biochar composites with variations of (150°C; 10 hours), (180°C; 10 hours), and (180°C; 12 hours) exhibit surface areas of 68.60 m^2/g, 103.16 m^2/g, and 101.51 m^2/g, respectively, while pure ZnO has a surface area of only 34.77 m^2/g. It has been demonstrated that the surfaces area of the ZnO-biochar composite can enhance the adsorption of organic pollutants, thereby leading to further improvement in photocatalytic performance [22]. Increasing the temperature from 150ºC to 180ºC during solvothermal synthesis results in a gradual enlargement of the pore structure within the composite, thereby increasing the pore density, and consequently, the surface area [23]. However, it is important to note that prolonged reaction times can result in particle agglomeration, an effect that can reduce the available surface area and potentially compromise photocatalytic efficiency [24].

Pore characteristics were analyzed using the Barrett-Joyner-Halenda (BJH) method to obtain the pore size distribution, pore volume, and micropore surface area of the samples [25]. These structural parameters are critical, as the pore size and its distribution within a photocatalyst directly affect the accessibility of active sites, which is a key factor in photodegradation performance [26]. This assertion is corroborated by the findings of He et al. (2015), who reported that enhanced photodegradation efficiency is associated with a broad pore size distribution and the presence of diverse pore types, particularly mesopores [27]. The identification of the pore characteristics of a material can be achieved through N_2 adsorption-desorption characterization using the BJH method, which generates isotherm type curves for the material [28]. The classification of the N_2 adsorption-desorption isotherm type curve can be determined based on the provisions of IUPAC (1985), as illustrated in Fig. 5 [29].

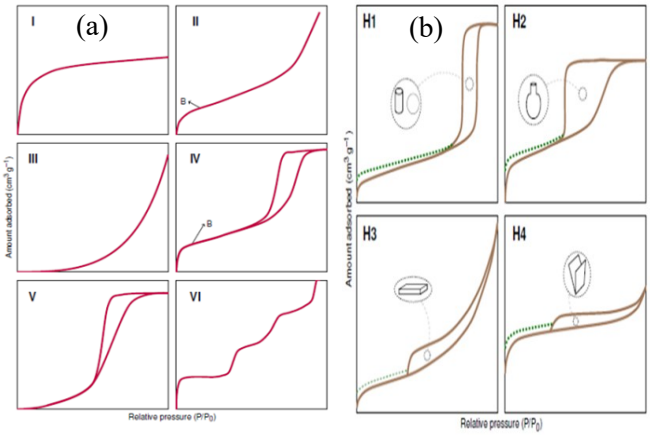

Fig. 5. (a) Physisorption isotherm type (b) Hysteresis loop type

The isotherm of type I curve indicates that the formed pores are of the micropore type, a state characterized by the absence of re-adsorption due to the surface of the micropores being filled by the adsorbate. In type II curves, the adsorption process occurs on nonporous powders or on powders with a larger diameter than micropores. Type III demonstrates an advanced adsorption process, whereby the interaction of the adsorbate with the adsorbed layer is greater than the interaction with the adsorbent surface. In addition, type IV curves are indicative of mesopores (20-500 Å) and are distinguished by the presence of hysteresis loops, resulting from disparities in the volume of adsorbed N_2 and desorbed N_2. The type V curve is a rare type, where the adsorbent and adsorbate interact weakly, while the type VI isotherm curve indicates a highly homogeneous interaction between the adsorbate and the adsorbent [29]. Fig. 6, illustrates the isotherm curve of the ZnO-biochar composites (180°C; 10 hours).

As demonstrated in Fig. 6, the results of the N_2 adsorption-desorption analysis indicate that the isotherm type of the ZnO-biochar composite material (180°C; 10 hours) is a type IV isotherm with an H3 hysteresis loop. The BET analysis exhibited that the ZnO-biochar composite at 180°C for 10

hours displayed an average pore diameter of 37.951 Å (3.8 nm). This finding suggests that the ZnO-biochar composite is a mesoporous material with a pore size ranging from 2 to 5 nm. All nanocomposites displayed typical type IV hysteresis loops, thereby confirming their mesoporous structures [30].

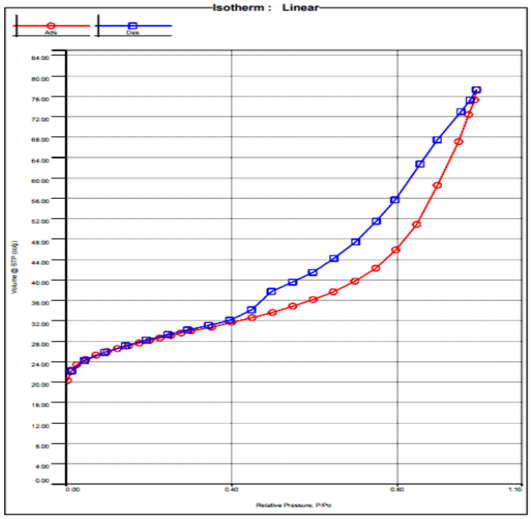

Fig. 6. N_2 adsorption-desorption isotherm curve of ZnO-biochar composite (180ºC; 10 hours)

3.2.3. *Fourier-transform infrared (FTIR) analysis*

Fourier Transform Infrared Spectroscopy (FTIR) is widely employed technique for determining molecular structure or chemical composition, particularly in the identification of characteristic functional groups and chemical bonds present in a composite or material. Furthermore, FTIR can provide detailed insights into interactions with other species based on the analysis of reactive peaks on the surface of the material. The FTIR spectrum of the ZnO-biochar composite synthesized at 180ºC for 10 hours is presented in Fig. 7.

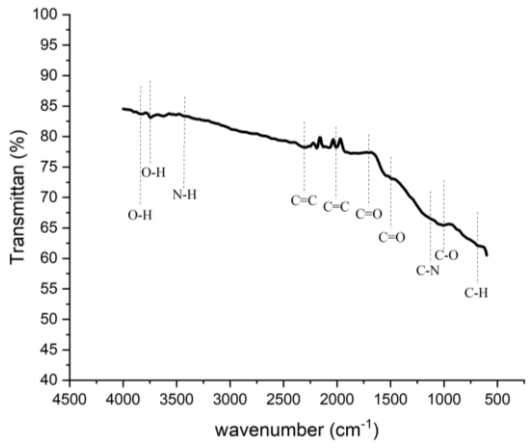

Fig. 7. FTIR analysis of the photocatalytic ZnO-biochar composite (180ºC; 10 hours)

The FTIR spectrum in Fig. 7 demonstrated a broad absorption band within the range of 3700-3584 cm^{-1}, which is indicative of O-H stretching vibrations [31]. This signal indicates the adsorption of water molecules onto the photocatalyst surface. These surface-bound –OH groups are significant, as they have the capacity to act as electron donors to the photoinduced holes, thereby generating hydroxyl radicals (•OH) that in turn drive the photocatalytic degradation process [32]. At 180°C, the O/N-H peak is located at 3420 cm^{-1}. In the wavelength range of 2500-2000 cm^{-1}, a C=C group is observed. At approximately 1720 cm^{-1}, a C=O group is detected. The C-O/N-C peak, which typically ranges from 1200-890 cm^{-1} manifests as a band and undergoes a shift to a higher wave number. This phenomenon is likely attributable to the conversion of sp3-C-O/N- to sp2-C-O/N- at elevated temperatures [20]. The peak at 755 cm^{-1} corresponds to the C-H aromatic group. The presence of -OH, C=C, C-N, and C-O groups as identified in the FTIR analysis indicates the functional groups found in N-graphene [33]. The peak observed at 420 cm^{-1} corresponds to the Zn-O group formed.

3.2.4. *X-Ray diffractometry (XRD) analysis*

X-Ray diffraction (XRD) is an analytical method used to identify the crystalline phase in materials by determining the parameters of the lattice structure and to obtain the particle size of the material. ZnO has three distinct morphologies: rocksalt, wurtzite, and cubic (zinc blende) structures. Of these, the wurtzite structure is considered to be the most stable [33]. The results of the analysis are presented in Fig. 8.

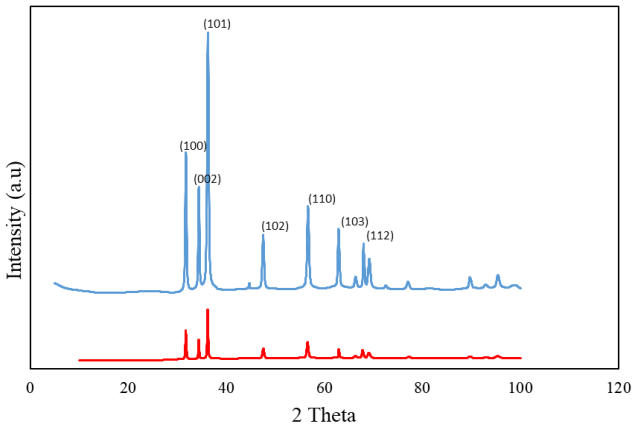

Fig. 8. XRD patterns of ZnO-biochar composites

XRD analysis is a method of determining the crystal structure in a solid sample. Fig. 8 demonstrates the XRD results of the material with a solvothermal time of 10 hours at 180°C and 10 hours at 150°C. ZnO-biochar exerts an hkl value that aligns with the characterization pattern of standard ZnO XRD analysis results (JCPDS No. 36-1451) at an angle of 36.207° and hkl (101). The ZnO peak value in the figure has an hkl value that is similar to the characterization pattern of the standard hexagonal wurtzite ZnO crystal, as determined by XRD analysis using JCPDS No. 36-1451, specifically (101), (002), (101), (102), (110), (103), and (112). The biochar peak is distributed on the ZnO crystal but exhibits a low intensity value. The ZnO-biochar composites display the same peak angles as (101), (002), (101), (102), (110), (103), and (112). The intensity of the composite peak increases with rising solvothermal temperature, indicating an enhancement in the crystallinity of the ZnO phase. The observed shift in the peak angle to 36.2° is indicative of distortion in the ZnO

lattice, which is concomitant with an expansion of the unit cell, a consequence of the strong interaction with ZnO and the carbon structure in biochar [20]. This research is consistent with the findings of Dumbrava's study, which indicates that elevated synthesis temperatures lead to enhanced crystallinity and increased crystal size [34].

It is evident that, in accordance with their constituent structure, solids can be categorized into two distinct classifications, namely crystals and amorphous. Crystalline solids are defined as those whose constituent particles (atoms) are arranged regularly to form three-dimensional structures and long-term regularity. Conversely, amorphous solids are characterized by a random arrangement of particles, leading to an absence of long-term regularity [35]. As demonstrated in Fig. 8, the presence of numerous peaks indicates the formation of a crystalinne structure in the ZnO-biochar composites. In the event of the material under scrutiny being crystalline, many peaks will manifest itself on the XRD graph. However, should the peak in question ne deemed non-existent, the material is classified as amorphous [36].

The average crystal size can be determined using the Debye-Scherrer equation [37].

$$D\ (nm) = \frac{K\lambda}{\beta \cos\theta} \quad (2)$$

where K represents Scherrer's constant (0.89), λ denotes the wavelength of the incident light (Cu, λ = 0.15406 nm), β is the full width at half maximum (FWHM), and θ corresponds to the diffraction angle. The crystal fraction of ZnO-biochar materials is presented in Table 3.

Table 3. Crystal fraction and size of materials

Material	Crystal size (nm)
*ZnO	38.7
ZnO-biochar (150ºC; 10 hours)	26.01
ZnO-biochar (180ºC; 10 hours)	27.28

(Source: *[20])

As illustrated in Table 3, the incorporation of biochar has been observed to result in a reduction in the crystallite size of ZnO. In terms of photocatalytic performance, a reduced crystallite size in the metal oxide typically leads to an increased number of voids, which serve as active sites for photocatalytic reactions. However, it is imperative to carefully optimize the crystallite size, as an excessive number of voids may increase charge recombination and consequently diminish the photocatalytic activity of the metal oxide. [38].

As depicted in Table 3, the crystal sizes of ZnO-biochar nanomaterials are synthesized at temperatures of 150°C and 180°C for 10 hours, from 19 to 37 nm, which corresponds to the size of active ZnO crystals [39]. The insignificant difference in solvothermal temperature has been demonstrated to have an insignificant effect on the crystal structure of ZnO-biochar composites [40]. Despite the occurrence of an increase in temperature during the solvothermal process, the resultant XRD analysis exhibited elevated intensity peaks, concomitant with an augmentation in crystal size [41]. As the intensity diffraction peaks increase, it is indicative of a high degree of integrity within the wurtzite crystal structure and high crystal purity [41].

3.2.5. *UV-Vis DRS analysis*

The band gap energy of the synthesized ZnO-biochar composite, a pivotal factor in its photocatalytic efficiency, was characterized through UV-Vis diffuse reflectance spectroscopy (UV-Vis DRS). The band gap is pivotal in dictating the wavelength-specific light absorption of a semiconductor, thereby exerting a fundamental control over the generation and separation of photogenerated charge carriers (electrons and holes) [42, 43]. Consequently, the electronic band structure is a critical factor influencing overall photocatalytic activity. The UV-Vis DRS spectrum, from which the band gap was derived, is shown in Fig. 9.

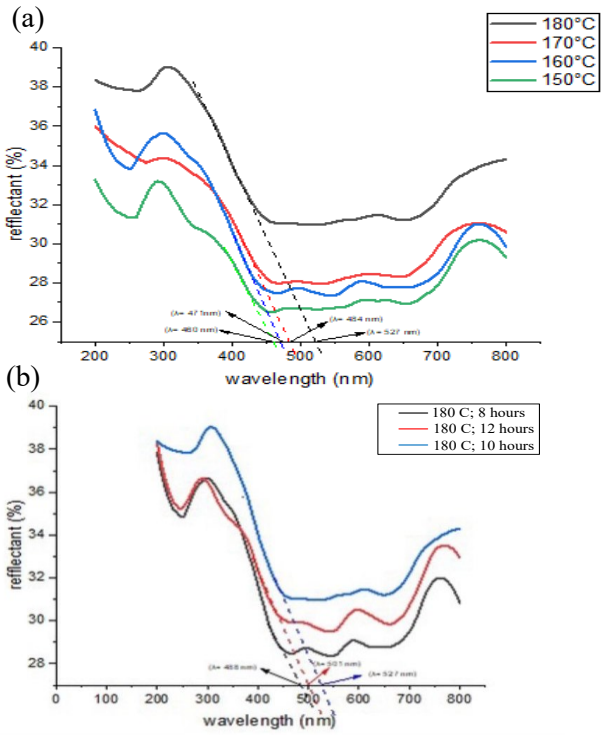

Fig. 9. UV-Vis DRS of the synthesized ZnO-biochar composites: (a) as a function of solvothermal temperature; (b) as a function of solvotermal reaction time

As demonstrated in Fig. 9, the UV-Vis DRS spectra plot reflectance (y-axis) against wavelength (x-axis). The analysis reveals that the ZnO-biochar composites exhibit a high degree of light absorption across a broad spectrum, ranging from approximately 420 to 800 nm. This demonstrates that the integration of palm shell-derived biochar extends the light-harvesting capability of the composite into the visible region. Fig. 9(a) further demonstrates that the absorption edges for composites synthesized at varying solvothermal temperatures are located at 527 nm (180ºC), 484 nm (170ºC), 471 nm (160ºC), and 460 nm (150ºC), indicating a progressive blue shift with decreasing temperature. Furthermore, the absorption peaks for each composite, based on differences in solvothermal reaction time, are recorded at 527 nm, 501 nm, and 488 nm for reaction times of 8 hours, 10 hours, and 12

hours, respectively. The light spectrum and its classification are illustrated in Fig. 10.

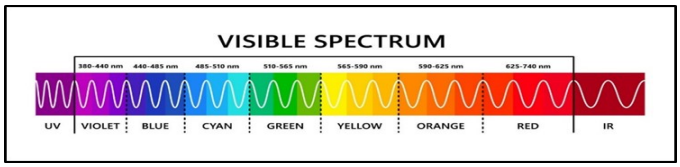

Fig. 10. The spectrum of light

The band gap energy can be calculated using the following equation [44].

$$E_g = h \times v = h \times \frac{c}{\lambda} \quad (3)$$

Description:
E = Energy (J) [1 Joule = 6.242x1019 eV]
h = Plank Constant (6.626x10-34 Js)
v = Radiation Frequency (s-1)
c = Speed of Light (3x108 m/s)
λ = Wavelength (nm)

The band gap energy value of the ZnO-biochar composites is presented in Table 4 and 5. The band gap value of each composite is illustrated Fig. 11.

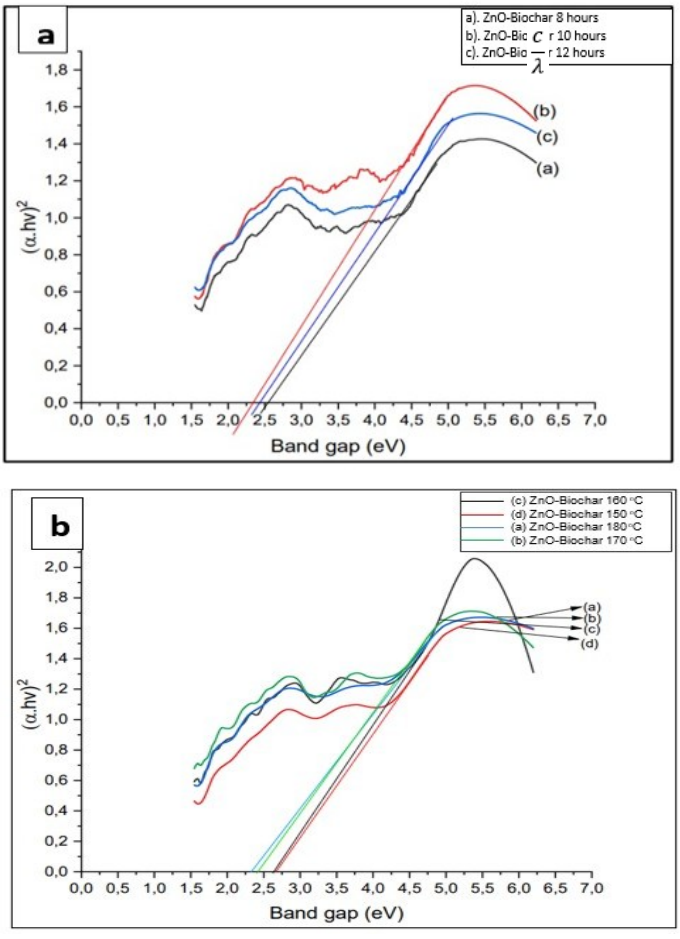

Fig. 11. Band gap value of ZnO-biochar composites with solvothermal (a) time variation at 180ºC; (b) temperature variation at 10 hours

Table 4. Band gap energy value of photocatalyst based on solvothermal temperature difference

Photocatalyst	Wavelength (nm)	Band gap energy Eg (eV)
ZnO-biochar (180˚C; 10 hours)	527	2.35
ZnO-biochar (170˚C; 10 hours)	484	2.56
ZnO-biochar (160˚C; 10 hours)	471	2.63
ZnO-biochar (150˚C; 10 hours)	460	2.69

Table 5. Band gap energy value of photocatalyst based on solvothermal time difference

Photocatalyst	Wavelength (nm)	Band gap energy Eg (eV)
ZnO-biochar (180˚C; 12 hours)	501	2.47
ZnO-biochar (180˚C; 10 hours)	527	2.35
ZnO-biochar (180˚C; 8 hours)	488	2.54

The band gap energy was obtained by means of the Tauc Plot method, which involved determining the optical band gap by analyzing the linear graph of the energy (eV) on the x-axis and (α.hv)1/n on the y-axis. The relationship between photon energy (hv) and the absorbance coefficient is described by the following equation.

$$(\alpha.hy)^{1/n} = c\ (hy\text{-}Eg) \quad (4)$$

In this equation, c represents the optical constant, α denotes the absorption coefficient, and (hv) signifies the photon energy. The variable Eg refers to the band gap energy, while n indicates the transition value, which varies depending on the type of transition: for direct transitions, n equals 1/2, and for indirect transitions, n equals 2 [45].

The graph of $(\alpha.hv)^2$ versus band gap (eV) is presented in Fig. 11, where the estimated band gap energy for ZnO-biochar composites ranges from 2.35 to 2.69 eV. As demonstrated in Fig. 11(a), the approximate band gap values of ZnO-biochar composites, with variations in solvothermal time at a constant temperature of 180°C, are 2.54 eV, 2.35 eV, and 2.47 eV for reaction times of 8 hours, 10 hours, and 12 hours, respectively. Meanwhile, Fig. 11(b) demonstrates the approximate band gap values for the temperature variation composite, with a constant reaction time of 10 hours, including 2.69 eV, 2.63 eV, 2.56 eV, and 2.35 eV for temperatures of 150°C, 160°C, 170°C, and 180°C, respectively. The incorporation of biochar into ZnO has been demonstrated to result in a narrowing of the band gap [20]. This phenomenon can be attributed to the expansion of light absorption from UV light to visible light, as well as increased light absorption, as demonstrated in the UV-Vis spectrum of DRS in Fig. 11 [20].

As demonstrated in Tables 4 and Table 5, the band gap energy of the ZnO-biochar composites is lower than that of pure ZnO, which is 3.37 eV [15]. The findings of this research suggest that the incorporation of graphene-like materials into the photocatalyst can result in a reduction of the band gap and the prevention of electron recombination. The decrease in band gap value is attributed to an increase in the particle size

of the composite, which is consistent with the results of the XRD analysis, indicating that the size of the composite at 180°C is larger than that at 150°C [40]. The incorporation of graphene-like material into the composite facilitates the formation of Zn-O-C bonds in the ZnO-biochar composites, resulting in the creation of new molecular orbitals and a decrease in band gap energy. A narrower band gap facilitates the generation of a greater number of electron-hole pairs, thereby enhancing photocatalytic activity [15].

The decrease in band gap value is attributed to an increase in the particle size of the composite, which aligns with the results obtained from the XRD analysis, indicating that the size of the composite at 180°C is larger than that at 150°C [40]. The incorporation of graphene-like material into the composite facilitates the formation of Zn-O-C bonds in the ZnO-biochar composites, resulting in the creation of new molecular orbitals and a decrease in the band gap energy. A smaller band gap energy has been shown to increase the number of hole-electron pairs, thereby enhancing photocatalytic activity [15].

As demonstrated in Fig. 11(b), the ZnO-biochar composites experience a wavelength shift towards the visible light, thereby affecting the band gap of the composite. The duration of the reaction time exerts a significant influence on the wavelength of the composite, a consequence of the accumulation of hydroxides along the grains of the ZnO-biochar composite and the topographical changes in ZnO that are the result of the extended reaction time [46]. The decrease in band gap resulting from an increase in solvothermal reaction time is attributed to a reduction in the surface area of the ZnO-biochar composites. This decrease in band gap, associated with prolonged reaction time, can lead to an increase in the size of the composite crystals due to the quantum size effect. In consideration to the findings, it can be concluded that a prolonged reaction time is conducive to the promotion of larger composite crystals and is concomitant with a reduction in structural defects. This defect reduction has been identified as the primary factor responsible for the observed increase in the band gap energy [46].

In consideration of the results obtained, it is evident that a solvothermal reaction time of 10 hours is identified as optimal. As demonstrated in Table 5, the extension of the duration to 12 hours results in an increase in the band gap value. While the composite's band gap generally decreased with longer reaction times, a slight increase was observed after surpassing the optimum duration [23]. This subsequent increase is attributed to excessive crystal growth at prolonged reaction times, which reduces structural defects and alters the electronic structure of the material [23].

4. Conclusion

The synthesis of a ZnO-biochar composite photocatalyst was achieved through the implementation of a combined solvothermal and calcination method. The material was comprehensively characterized using SEM-EDX, BET, XRD, and UV-Vis DRS. Methylene blue was utilized as a model contaminant to assess the degradation efficiency of the ZnO-biochar composites. The methylene blue degradation configuration employs a mercury lamp as the light source. The highest degradation of methylene blue was observed in the ZnO-biochar composite synthesized at a solvothermal temperature of 180°C and a reaction time of 10 hours, achieving a degradation yield of 88.29%. The ZnO-biochar composite exhibiting the most effective methylene blue degradation possesses characteristics including a spherical and porous morphology, functional groups indicated by absorption peaks, a crystal size of 27.28 nm, a surface area of 103.16 m2/g, a diameter size of 37.951 Å (3.8 nm), and a band gap energy of 2.35 eV.

Acknowledgements

This present work has been supported by the Ministry Education, Culture, Research and Technology, the Republic of Indonesia, through Fundamental-Regular (PFR) scheme (contract number:19514/UN19.5.1.3/AL.04/2025;102/C3/DT.05.00/ PL /2025).

References

1. Wang, X. Q., S. F. Han, Q. W. Zhang, N. Zhang, dan D. D. Zhao., *Photocatalytic oxidation degradation mechanism study of methylene blue dye wastewater with GR/iTO₂*, MATEC Web of Conferences. 238 (2018) 03006.
2. Agustania, A. A., *Aktivitas Fotokatalis Nano TiO₂ Terimobilisasi Membran Poliuretan dalam Reaksi Fotodegradasi Zat Warna Metilen Biru*, Disertasi Doktor, UIN Ar-Raniry Fakultas Sains dan Teknologi. (2022).
3. Oladoye, Peter Olusakin, Timothy Oladiran Ajiboye, Elizabeth Oyinkansola Omotola, and Olusola Joel Oyewola., *Methylene blue dye: Toxicity and potential elimination technology from wastewater,* Results in Engineering. 16 (2022).
4. J. S. Miranda, N. C. A. Silva, J. J. Bassi, M. C. C. Corradini, F. A. P. Lage, D. B. Hirata, and A. A. Mendes, Immobilization of Thermomyces lanuginosus lipase on mesoporous poly-hydroxybutyrate particles and application in alkyl esters synthesis: Isotherm, thermodynamic and mass transfer studies, Chem. Eng. J. 251 (2014) 392–403.
5. He, K., C. Zhao, G. Zhao, dan G. Han., *Effects of pore size on the photocatalytic activity of mesoporous TiO₂ prepared by a sol–gel process*, Journal of Sol-Gel Science and Technology. 75 (2015) 557–563.
6. Yu, S., J. Zhou, Y. Ren, Z. Yang, M. Zhong, X. Feng, B. Su, dan Z. Lei., *Excellent adsorptive–photocatalytic performance of zinc oxide and biomass-derived N,O-contained biochar nanocomposites for dyes and antibiotic removal*, Chemical Engineering Journal. 451 (2023) 138959.
7. Setyawan, D., dan P. Handoko., *Aktivitas katalis Cr/Zeolit dalam reaksi konversi katalitik fenol dan metil isobutil keton*, Jurnal Ilmu Dasar. 4 (2003) 73–76.
8. Hidayati, U. F., A. B. Aritonang, dan L. Destiarti., *TiO₂-rGO Composite for Photocatalytic Decolorization of Methylene Blue Under the Visible Light Illumination*, BERKALA SAINSTEK. 9 (2021) 167–173.
9. Harris, K., J. Gaskin, M. Cabrera, W. Miller, dan K. C. Das., *Characterization and mineralization rates of low temperature peanut*

hull and pine chip biochars, Agronomy. 3 (2013) 294–312.
10. Natarajan, S., H. C. Bajaj, dan R. J. Tayade., *Recent advances based on the synergetic effect of adsorption for removal of dyes from wastewater using photocatalytic process*, Journal of Environmental Sciences. 65 (2018) 201–222.
11. Hameed, B. H., A. M. Din, dan A. L. Ahmad., *Adsorption of methylene blue onto bamboo-based activated carbon: kinetics and equilibrium studies*, Journal of Hazardous Materials. 141 (2007) 819–825.
12. Shrestha, P., M. K. Jha, J. Ghimire, A. R. Koirala, R. M. Shrestha, R. K. Sharma, B. Pant, M. Park, H. R. Pant., *Decoration of zinc oxide nanorods into the surface of activated carbon obtained from agricultural waste for effective removal of methylene blue dye*, Materials. 13 (2020) 5667.
13. Jing, H., L. Ji, Z. Wang, J. Guo, S. Lu, J. Sun, L. Cai, dan Y. Wang., *Synthesis of ZnO nanoparticles loaded on biochar derived from Spartina alterniflora with superior photocatalytic degradation performance*, Nanomaterials. 11 (2021) 2479.
14. Tsai, W. T., C. Y. Chang, dan S. L. Lee., *Preparation and characterization of activated carbons from corn cob*, Carbon. 35 (1997) 1198–1200.
15. Luo, H., S. Yu, M. Zhong, Y. Han, B. Su, dan Z. Lei., *Waste biomass-assisted synthesis of TiO_2 and N/O-contained graphene-like biochar composites for enhanced adsorptive and photocatalytic performances*, Journal of Alloys and Compounds. 899 (2022) 163287.
16. Liew, R. K., M. Y. Chong, O. U. Osazuwa, W. L. Nam, X. Y. Phang, M. H. Su, C. K. Cheng, C. T. Chong, dan S. S. Lam., *Production of activated carbon as catalyst support by microwave pyrolysis of palm kernel shell: a comparative study of chemical versus physical activation*, Research on Chemical Intermediates. 44 (2018) 3849–3865.
17. Hou, J., J. Yun, W. Jang, J. H. Kim, dan H. Byun., *Polyacrylonitrile nanofiber membranes incorporated with large reduced graphene oxide content in situ*, Journal of Materials Science. 56 (2021) 18508–18521.
18. Seal, K., H. Chaudhuri, S. Basu, M. K. Mandal, dan S. Pal., *Study on effect of the solvothermal temperature on synthesis of 3D hierarchical TiO_2 nanoflower and its application as photocatalyst in degradation of organic pollutants in wastewater*, Arabian Journal for Science and Engineering. 46 (2021) 6315–6331.
19. Paszkiewicz-Gawron, M., A. Gołąbiewska, A. Pancielejko, W. Lisowski, J. Zwara, M. Paszkiewicz, A. Zaleska-Medynska, dan J. Łuczak., *Impact of tetrazolium ionic liquid thermal decomposition in solvothermal reaction on the remarkable photocatalytic properties of TiO_2 particles*, Nanomaterials. 9 (2019) 744.
20. Iasya, Y. K., F. Khoerunnisa, S. S. Dwi, R. A. Putri, M. Nurhayati, U. S. Arrozi, Y. Permana, M. Handayani, W. D. Astuti, O. W. Da, dan I. Irnanda., *Synergetic effect of ZnO/NiO nanocomposite on the enhancement of photocatalytic degradation efficiency of dyes molecules*, Communications in Science and Technology. 10 (2025) 1–9.
21. Leichtweis, J., S. Silvestri, dan E. Carissimi., *New composite of pecan nutshells biochar–ZnO for sequential removal of acid red 97 by adsorption and photocatalysis*, Biomass and Bioenergy. 140 (2020) 105648.
22. Yu, S., J. Zhou, Y. Ren, Z. Yang, M. Zhong, X. Feng, B. Su, dan Z. Lei., *Excellent adsorptive–photocatalytic performance of zinc oxide and biomass-derived N,O-contained biochar nanocomposites for dyes and antibiotic removal*, Chemical Engineering Journal. 451 (2023) 138959.
23. Xue, B., dan Y. Zou., *High photocatalytic activity of ZnO–graphene composite*, Journal of Colloid and Interface Science. 529 (2018) 306–313.
24. Tian, F., R. Zhu, K. Song, M. Niu, F. Ouyang, dan G. Cao., *The effects of hydrothermal temperature on the photocatalytic performance of $ZnIn_2S_4$ for hydrogen generation under visible light irradiation*, Materials Research Bulletin. 70 (2015) 645–650.
25. Palharim, P. H., M. C. Caira, C. de Araújo Gusmão, B. Ramos, G. T. dos Santos, O. Rodrigues Jr., dan A. C. Teixeira., *Effect of temperature and time on the hydrothermal synthesis of WO_3–AgCl photocatalysts regarding photocatalytic activity*, Chemical Engineering Research and Design. 188 (2022) 935–953.
26. He, K., C. Zhao, G. Zhao, dan G. Han., *Effects of pore size on the photocatalytic activity of mesoporous TiO_2 prepared by a sol–gel process*, Journal of Sol-Gel Science and Technology. 75 (2015) 557–563.
27. Bardestani, R., G. S. Patience, dan S. Kaliaguine., *Experimental methods in chemical engineering: specific surface area and pore size distribution measurements — BET, BJH, and DFT*, The Canadian Journal of Chemical Engineering. 97 (2019) 2781–2791.
28. IUPAC, S. K. Sing., *Reporting physisorption data for gas/solid systems with special reference to the determination of surface area and porosity (Recommendations 1984)*, Pure and Applied Chemistry. 57 (1985) 603–619.
29. Zhang, Y., J. Zhou, X. Chen, Q. Feng, dan W. Cai., *MOF-derived C-doped ZnO composites for enhanced photocatalytic performance under visible light*, Journal of Alloys and Compounds. 777 (2019) 109–118.
30. Agusriyanti, S., dan P. Artsanti., *Pemanfaatan Zeolit Alam Ciamis sebagai Pengemban Fotokatalis TiO_2 untuk Fotodegradasi Zat Warna Rhodamin B*, Jurnal Sains Dasar. 4 (2015) 92–99.
31. Linsebigler, A. L., G. Lu, dan J. T. Yates Jr., *Photocatalysis on TiO_2 surfaces: principles, mechanisms, and selected results*, Chemical Reviews. 95 (1995) 735–758.
32. Sudhakar, S., K. K. Jaiswal, S. G. Peera, dan A. P. Ramaswamy., *Green synthesis of N-graphene by hydrothermal-microwave irradiation for alkaline fuel cell application*, International Journal of Recent Scientific Research. 8 (2017) 19049–19053.
33. Dumbrava, A., C. Matei, A. Diacon, F. Moscalu, D. Berger., *Novel ZnO-biochar nanocomposites obtained by hydrothermal method in extracts of Ulva lactuca collected from Black Sea*, Ceramics International. 49 (2023) 10003–10013.
34. Anjarkusuma, D. I., *Struktur, komposisi kimia, dan morfologi permukaan bahan semikonduktor paduan Sn dengan variasi lama pemanasan hasil preparasi dengan teknik Bridgman*, 2017.
35. Pratiwi, P. D., *Preparasi Nanomaterial Karbon Menggunakan Metode Liquid Mechanical Exfoliation Dibantu oleh Linear Alkylbenzene Sulfonate dengan Variasi Waktu Pencampuran*, Skripsi S1, FMIPA UNY. 2016.
36. Bouanimba, N., N. Laid, R. Zouaghi, T. Sehili., *A comparative study of the activity of TiO_2 Degussa P25 and Millennium PCs in the photocatalytic degradation of bromothymol blue*, International Journal of Chemical Reactor Engineering. 16 (2018).
37. Thongjamroon, S., J. Wootthikanokkhan, dan N. Poolthong., *Photocatalytic performances and antifouling efficacies of alternative marine coatings derived from polymer/metal oxides (WO_3@TiO_2)-based composites*, Catalysts. 13 (2023) 649.
38. Humadi, J., A. T. Nawaf, L. A. Khamees, Y. A. Abd-Alhussain, H. F. Muhsin, M. A. Ahmed, dan M. M. Ahmed., *Development of new effective activated carbon supported alkaline adsorbent used for removal of phenolic compounds*, Communications in Science and Technology. 8 (2023) 164–170.
39. Tian, F., R. Zhu, K. Song, M. Niu, F. Ouyang, dan G. Cao., *The effects of hydrothermal temperature on the photocatalytic performance of $ZnIn_2S_4$ for hydrogen generation under visible light irradiation*, Materials Research Bulletin. 70 (2015) 645–650.
40. ElFaham, M. M., A. M. Mostafa, dan E. A. Mwafy., *The effect of reaction temperature on structural, optical and electrical properties of tunable ZnO nanoparticles synthesized by hydrothermal method*, Journal of Physics and Chemistry of Solids. 154 (2021) 110089.
41. Josun, J., P. Sharma, dan V. K. Garg., *Optical and structural behavior of hydrothermally synthesized ZnO nanoparticles at various temperatures with NaOH molar ratios*, Results in Optics. 14 (2024) 100601.
42. Lestari, D., W. Sunarto, dan E. B. Susatyo., *Preparasi Nanokomposit ZnO/TiO_2 dengan Sonokimia serta Uji Aktivitasnya untuk Fotodegradasi Fenol*, Indonesian Journal of Chemical Science. 1 (2012).
43. Muthirulan, P., C. N. Devi, dan M. M. Sundaram., *TiO_2 wrapped graphene as a high performance photocatalyst for acid orange 7 dye*

degradation under solar/UV light irradiations, Ceramics International. 40 (2014) 5945–5957.

44. Rini, A. S., A. H. Sitorus, Y. Rati, E. Taer, Z. Usman, dan A. A. Umar., *Biosynthesis of sulfur and selenium co-doped ZnO nanoparticles for the enhanced photocatalytic treatment of industrial wastewater*, Communications in Science and Technology. 10 (2025) 10–16.
45. Ali, M. M., *Characterization of ZnO thin films grown by chemical bath deposition*, Journal of Basrah Researches (Sciences). 37 (2011).